A low-temperature extended X-ray absorption study of the local order in simple and complex perovskites. II. PMN ($PbMg_{1/3}Nb_{2/3}O_3$)

1993 J. Phys.: Condens. Matter 5 4889

(http://iopscience.iop.org/0953-8984/5/28/005)

J. Phys.: Condens. Matter 5 (1993) 4889–4902. Printed in the UK

A low-temperature extended x-ray absorption study of the local order in simple and complex perovskites: II. PMN ($PbMg_{1/3}Nb_{2/3}O_3$)

E Prouzet†, E Husson‡§¶, N de Mathan‡ and A Morell‖

† Laboratoire de Chimie des Solides, Institut des Matériaux, CNRS UMR 110, 2 rue de la Houssinière, 44072 Nantes Cédex 03, France

‡ Laboratoire de Chimie Physique du Solide, URA CNRS 453, Ecole Centrale de Paris, 92295 Chatenay-Malabry Cédex, France

§ Laboratoire de Physique et Mécanique des Matériaux, ESEM, Université d'Orléans and CRPHT-CNRS, 45071 Orléans Cédex, France

‖ THOMSON-CSF, LCR, Domaine de Corbeville, 91401 Orsay Cédex, France

Received 24 February 1993

Abstract. An EXAFS study of lead magnesium niobate was performed at the Nb K edge and at the Pb L_{III} edge between 300 and 4.5 K. Two Nb–O bond lengths of 1.95 and 2.16 Å are observed and there is no significant modification of the local environment of the Nb atoms with temperature. The distribution of these two bonds in both polar nanodomains and 1–1 Nb–Mg ordered nanodomains is discussed in relation to results obtained previously by other techniques. It is shown that the ordered nanodomains could occupy about one third of the whole volume. The results obtained for the Nb–Nb and Nb–Mg distances confirm the structural results and particularly point to an increasing correlation of the Nb shift at their site, when the temperature is lowered to below 300 K. The weak EXAFS signal obtained at the Pb L_{III} edge and the small backscattered contribution of Pb at the Nb K edge reveal a strong static disorder of the Pb positions.

1. Introduction

In a recent paper [1] we have presented the EXAFS study of potassium niobate performed at the Nb K edge between 300 and 4.5 K. It was shown that, at short range, in the rhombohedral phase ($T < 263$ K), the Nb shift along one [111] direction of the basis cube, within its oxygen octahedron considered as rigid, originates three short Nb–O bonds and three longer ones. In this case, the local position detected by EXAFS and the average position determined by x-ray or neutron diffraction are the same. In contrast, in the orthorhombic phase (263 K $< T <$ 498 K), the EXAFS study shows that the Nb cation shift is identical to that of the rhombohedral phase, whereas, for studies using long-range techniques, the average position of the Nb appears as a shift along a [110] axis. So this work gave direct confirmation of the 'eight-site model' [2–4] and thus of the order–disorder character of the phase transitions in ferroelectric perovskites such as $KNbO_3$. In this paper, we present the EXAFS results obtained for the complex perovskite $PbMg_{1/3}Nb_{2/3}O_3$ (PMN) between 300 and 4.5 K, in comparison with $KNbO_3$ taken as reference.

$PbMg_{1/3}Nb_{2/3}O_3$ has been studied at temperatures from 700 to 4 K by powder x-ray and neutron diffraction [5–7] as well as by room temperature x-ray diffraction on a single crystal

¶ To whom correspondence should be addressed.

0953-8984/93/284889+14$07.50

[8]. At 20 °C, the average structure of PMN is cubic (space group $Pm3m$, $a = 4.044$ Å) with atoms statistically shifted off their special positions. The disordered local positions and the isotropic thermal parameters of Pb and O atoms were defined. But the Nb/Mg atomic shifts could not be determined precisely because they are small and strongly correlated with the $B_{Nb/Mg}$ thermal parameters.

At low temperature, the atomic shifts, which were random at high temperature, would become correlated from one cell to another one, originating very small polar regions characterized by antiparallel shifts of the cations against oxygen atoms. The best structural fit was obtained with shifts along the [111] direction of the cube, leading to a local rhombohedral symmetry. The nucleation of the polar regions begins at about 600 K. Their correlation length increases with the lowering of temperature and it was evaluated to be about 100 Å at 5 K. Due to local variations of polarization, two phases seem to coexist in the crystal at 5 K: a polar phase, which has been roughly evaluated at 20%, and a non-polar phase associated with host lattice. The polar region growth should be inhibited by the existence of domains of about 20 Å size in which the Nb(V) and Mg(II) cations are 1–1 ordered on the B site of the perovskite [9]. Taking into account the small size of both polar and ordered nanodomains, the long-range structure remains roughly cubic in the whole temperature range. The existence of polar domains is only revealed in the powder x-ray and neutron diffraction patterns by diffuse scattering increasing when the temperature is lowered [7], and the 1–1 ordered domains are only revealed on the electron diffraction patterns by superstructure spots at positions $h + \frac{1}{2}, k + \frac{1}{2}, l + \frac{1}{2}$ [10].

Finally, Raman spectroscopy studies [11, 12] allowed the characterization of the chemical bonds in PMN: the Nb–O bonds sharing their O atom with Mg are strengthened and exhibit a vibration range at about 780 cm^{-1}, whereas the Nb–O bonds sharing their O atom with another Nb exhibit a vibration range at about 500 cm^{-1}. This latter presents two maxima that reveal the existence of two Nb–O bond lengths and thus Nb–O polar bonds at temperatures above the maximum of the permittivity ($T_{max} = 270$ K). The Mg–O bonds are revealed by a weak intensity line at about 450 cm^{-1} [11]. On the other hand, polarized Raman spectra have shown the existence of 1–1 ordered regions with an $Fm3m$ structure [12].

This EXAFS study was thus undertaken in order to complete the data on the short-range order in PMN and to define the Nb local environment.

2. Experimental details

2.1. EXAFS measurements

The spectra have been recorded at DCI, in the French Synchrotron Laboratory LURE, by using the EXAFS IV spectrometer, mounted with a two-crystal Si(331) monochromator. During the experiments, the storage ring used 1.85 GeV positrons with a 250 mA average intensity. Data were collected in transmission mode by the measurement of the beam intensities I_0 and I, respectively before and after introduction of the sample, using ion chambers with argon fill gas.

Samples were prepared from 20 μm gain size powders trapped in a nylon weave, then recorded at 300, 230, 100 and 4.5 K, at the Nb K edge, from 18 850 to 19 850 eV (3 eV steps) and at the lead L_{III} edge, from 12 900 to 13 900 eV (2 eV steps), with 1 s accumulation time per point.

2.2. *Data processing*

2.2.1. Niobium K edge. The atomic absorption above the edge was approximated by a fifth-degree polynomial expression from 19 008 to 19 850 eV. The EXAFS contribution was then extracted between 19 010 and 19 850 eV with E_0 taken equal to the energy at half the edge jump, 18 986 eV. A Kaiser window ($\tau = 3.5$) extending from $k = 2.8$ up to 14.0 $Å^{-1}$ ($E \simeq 30$–750 eV) was then applied to the $k^n\chi(k)$ ($n = 1$ or 2 for the O and Nb shells respectively) weighted data before Fourier transformation.

A removal of the low-range waves and noise has been performed through a 1–10 Å back Fourier transform, then a 2.8–14 $Å^{-1}$ Fourier transform. All the moduli curves of the Fourier transforms—called RDF—are not phase-shift corrected and are so pseudo-radial distribution functions.

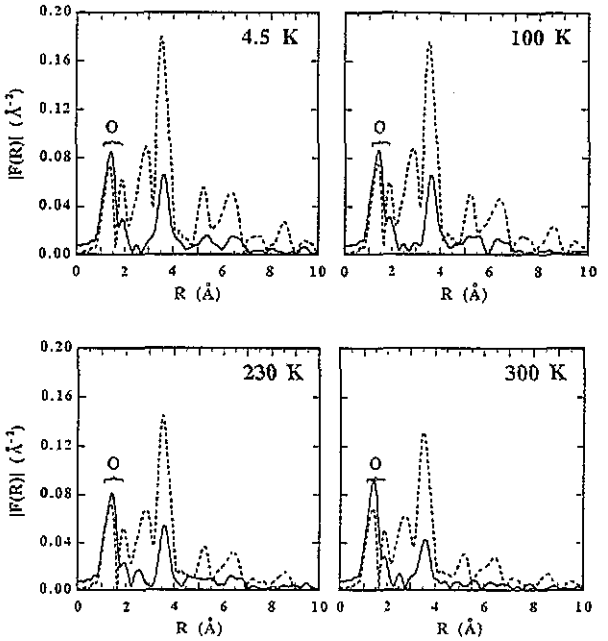

Figure 1. RDF (uncorrected for phase shift) of the niobium K edge $k\chi(k)$ EXAFS spectra for the 300, 230, 100 and 4.5 K samples, for PMN (——) compared to $KNbO_3$ (– – –). The RDF exhibits the two O shells and the first Nb shell. The Pb shell, which should peak around 3 Å, does not appear, even at 4.5 K.

2.2.2. Lead L_{III} edge. The atomic absorption was approximated by a fifth-degree polynomial expression from 13 050 to 13 900 eV. The EXAFS contribution was extracted between 13 055 and 13 900 eV with E_0 taken equal to the energy at half the edge jump, 13 036 eV. A Kaiser window ($\tau = 2.5$) extending from $k = 2.6$ up to 15.0 $Å^{-1}$ ($E \simeq 25$–850 eV) was then applied to the $k^3\chi(k)$ weighted data before Fourier transformation. These RDFs are also not phase-shift corrected.

The EXAFS analysis has been described previously [1]. The various shells have been firstly extracted by a back Fourier transform including a removal of the Kaiser window contribution, then studied through a fitting procedure using Teo and Lee's tabulated [13] amplitudes and phase shifts. The back Fourier transformed contributions of each of the various shells have been analysed through the classical EXAFS formula based on the plane wave single-scattering theory, expressed by the equation

$$k\chi(k) = -S_0^2 \sum_i \frac{N_i}{R_i^2} \exp(-2k^2\sigma_i^2) \exp(-2R_i\Gamma/k) f_i(\pi, k) \sin[2kR_i + \Phi_i(k)].$$

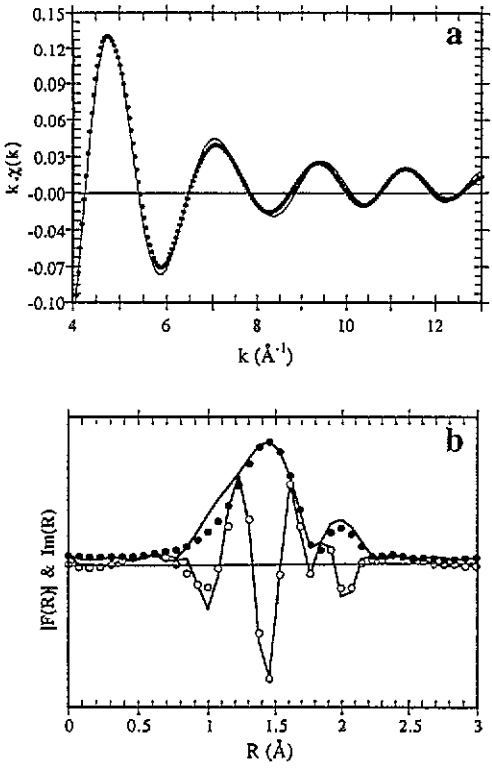

Figure 2. Simulated spectra for the two O shells of the PMN (4.5 K) $k\chi(k)$ EXAFS spectrum: (*a*) EXAFS spectrum (——, experimental; ●, calculated); (*b*) Fourier transform (——, experimental modulus and imaginary part; ●, calculated modulus; ○, calculated imaginary part).

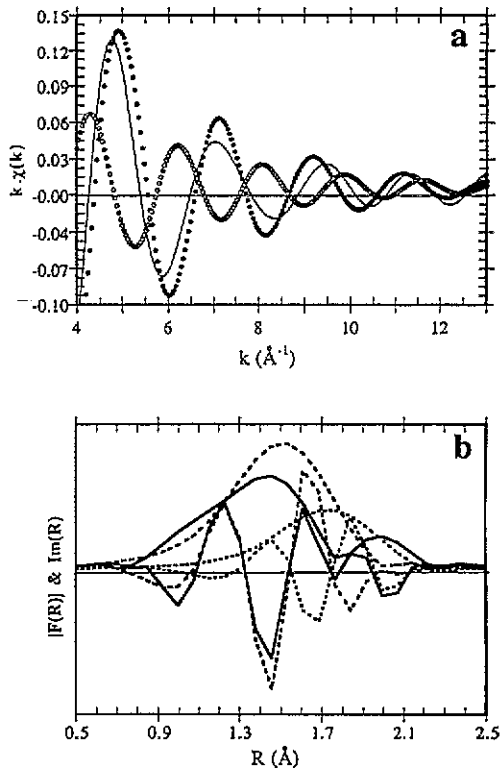

Figure 3. Comparison between the simulated spectra for each O shell of the PMN (4.5 K) $k\chi(k)$ EXAFS spectrum with the experimental one. (*a*) EXAFS spectrum: the experimental spectrum looks like a single-shell contribution because the two simulated EXAFS spectra corresponding to each oxygen shell are out of phase. (——, experimental; ●, calculated for the first shell (R_{O1} = 1.95 Å); ○, calculated for the second shell (R_{O2} = 2.16 Å).) (*b*) Fourier transform: the RDFS of the two simulated O single shells do not peak at the same distance and with the same intensity as the experimental one because real and imaginary parts interfere. (——, experimental modulus and imaginary part; - - - -, calculated modulus and imaginary part for each O shell.)

When theoretical amplitude and phase shift files are used, S_0 and Γ can be basically considered like agreement factors. Therefore they were not allowed to vary for the whole series of samples, but were kept equal to those determined for our previous $KNbO_3$ study in order to allow comparison with our results [1].

The quality of the fit is determined by both the error factor ρ and χ^2:

$$\rho = \sum_k k^{2q}[k\chi_{\text{exp}}(k) - k\chi_{\text{theo}}(k)]^2 \Big/ \sum_k k^{2q}[k\chi_{\text{exp}}(k)]^2$$

$$\chi^2 = \sum_k k^{2q}[k\chi_{\text{exp}}(k) - k\chi_{\text{theo}}(k)]^2.$$

Table 1. Results of the fits for the two O coordination shells. N_{Oi} and R_{Oi} represent respectively the number of O atoms and the distances Nb–O for the ith shell. σ_i and ΔE_i^0 are the Debye–Waller factor and the energy shift versus the experimental K Nb edge. ρ and χ^2 are error factors. The fitting is performed with Teo and Lee's tabulated amplitude and phase shift files; S_0 (the scale factor) and Γ ($\Gamma = k/\lambda$ where λ is the electronic mean free path) are respectively fixed at 0.8 and 0.91 Å^{-2}.

	300 K	230 K	100 K	4.5 K
Oxygen 1				
N_1	4.0	3.9	4.0	4.1
R_1 (Å)	1.95	1.95	1.94	1.95
σ_1 (Å)	0.065	0.070	0.070	0.071
ΔE_1^0 (eV)	13.4	13.3	13.0	13.8
Oxygen 2				
N_2	2.0	2.1	2.0	1.9
R_2 (Å)	2.15	2.17	2.15	2.16
σ_2 (Å)	0.054	0.074	0.059	0.056
ΔE_2^0 (eV)	11.6	13.1	12.9	12.8
ρ (%)	0.9	1.1	1.7	1.2
χ^2	0.7×10^{-3}	0.7×10^{-3}	1.3×10^{-3}	0.9×10^{-3}

The q parameter was chosen as 0.5 for this study.

3. Results and discussion

3.1. Niobium K edge

Figure 1 compares the 300, 230, 100 and 4.5 K RDFs of PMN with the $KNbO_3$ values. The two first peaks (1.5 and 2.0 Å) correspond to the octahedral O environment and the other peak (3.6 Å) is due to the Nb atoms in the six closest octahedra. If we compare these spectra to the $KNbO_3$ ones, we see that the peak which would have to appear at almost the same distance as the K neighbours in the $KNbO_3$ structure (~ 3 Å) is not observed, even at 4.5 K. It can be observed also (i) that the Nb peak is much less intense than the analogous peak for $KNbO_3$, and (ii) that the peaks corresponding to the outer shells do not appear.

3.1.1. The oxygen shell. All the RDFs exhibit two peaks, which are attributed to the backscattering of the first O neighbours; they have approximately the same profiles and the same intensities whatever the temperature. This shows that two types of Nb–O distance exist in the rhombohedral phase as well as in the orthorhombic phase. We have performed fits between 2.8 and 14.0 Å^{-1} on $k\chi(k)$ EXAFS spectra from a back Fourier transform taken from 1.07 to 2.10 Å. We took the same value as in our previous study for Γ ($\Gamma_1 = \Gamma_2 = 0.91$ Å^{-2}) and the scale factor ($S_0 = 0.8$) [1]. The spectra were fitted by using the condition ($N_{O1} + N_{O2} = 6$).

The results, given in table 1 and figure 2, show that N_{O1} and N_{O2} are respectively close to four and two and that the small variations of σ_{O1} and σ_{O2} from 4.5 to 300 K cannot be assigned to a physical phenomenon. Actually, the results must be carefully considered because the two contributions interfere as is shown in figure 3(a): as the two simulated EXAFS spectra corresponding to each O shell are out of phase, the experimental spectrum looks like a single-shell contribution (there is not a beat node as observed for $KNbO_3$ [1]).

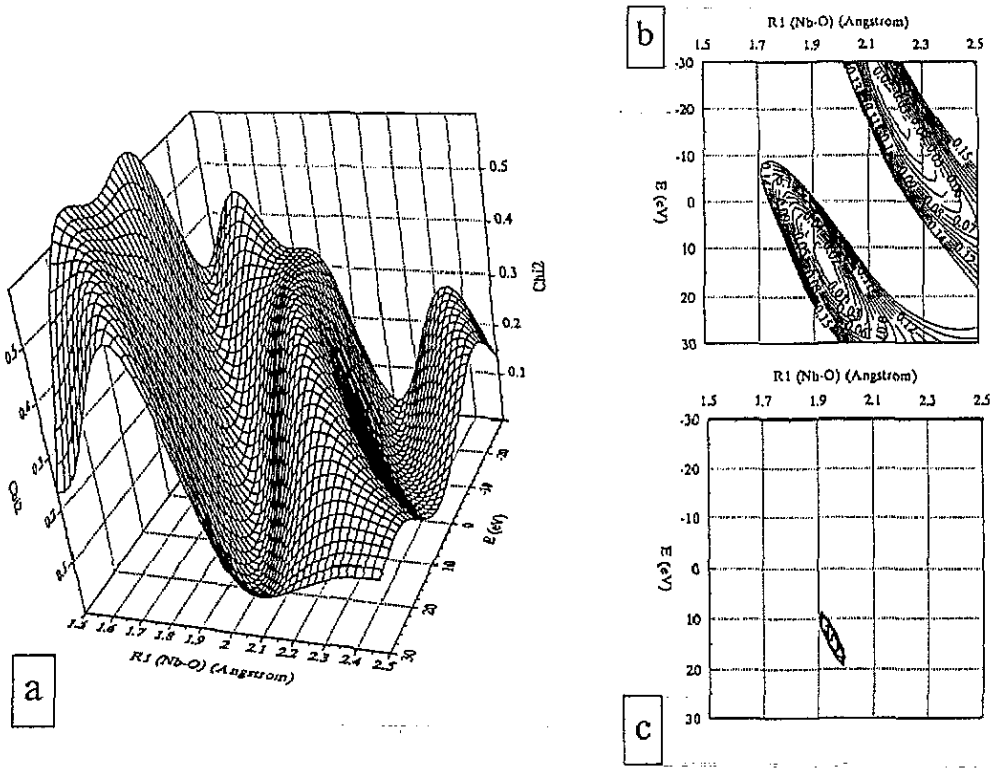

Figure 4. (*a*) Evolution of the χ^2 factor with variation of the distance R_1 and the edge shift E for the first O shell (R_1 from 1.5 to 2.5 Å and E from −30 to 30 eV); (*b*) map of the 0.01 step variations of χ^2; (*c*) map of the χ^2 values lower than 0.01.

For the same reason, it can be seen in figure 3(*b*) that the RDFs of the two simulated O single shells do not peak at the same distance and with the same intensity as the experimental one because real and imaginary parts interfere. On the other hand, it is well known that some parameters of the EXAFS formula are highly correlated: for instance, if N_{Oi} and σ_{Oi} are allowed to vary together, meaningless evolution often occurs because they can undergo mathematical random deviations and cancel each other. For analogous reasons, even if the distance R_i and ΔE_i^0—the edge variation from the theoretical value of the references—are not so linked usually, for our particular case (where the two EXAFS signals strongly interfere), the mathematical treatment could lead to values further from the real ones. This is why we had first to check the validity of the values found by EXAFS. These calculations have been performed for the 4.5 K sample: we let two parameters vary, the others being kept fixed and equal to the values given in table 1.

Figure 4 presents the variations of χ^2 as a function of R_1 and ΔE_1^0 and figure 5 presents the variations of χ^2 as a function of R_2 and ΔE_2^0. It is confirmed that the mathematical values previously found can be assigned to a true minimum of the χ^2 factor, even if we can find a correlation in the range (1.90–2.00 Å; 10–20 eV) for (R_1; ΔE_1^0) and a stronger one in the range (2.10–2.20 Å; 7–17 eV) for (R_2; ΔE_2^0). As the average precision in the distances is about 0.02 Å, these figures confirm that a few eV variation of ΔE^0 does not actually

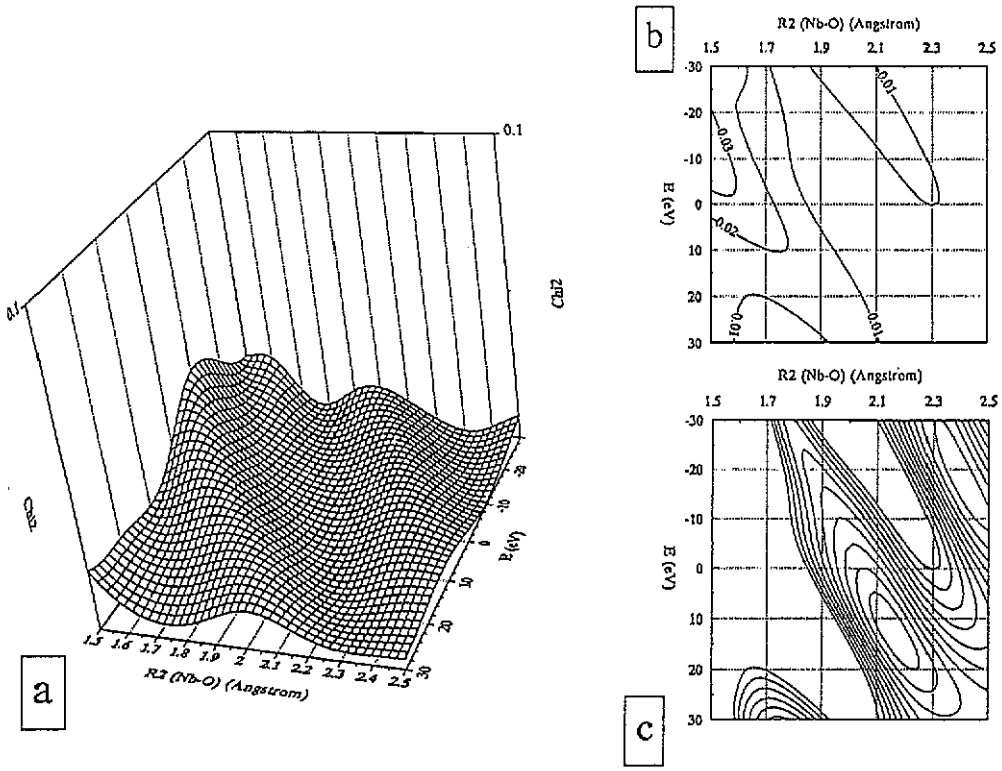

Figure 5. (*a*) Evolution of the χ^2 factor with variation of the distance R_2 and the edge shift E for the second O shell (R_2 from 1.5 to 2.5 Å and E from −30 to 30 eV); (*b*) map of the 0.01 step variations of χ^2; (*c*) map of the χ^2 values lower than 0.01.

affect the result concerning the distance. We carried out the same calculation for the set (R_1, R_2) (figure 6): a wrong minimum can be seen around $R_1 = 2.05$ Å, $R_2 = 1.85$ Å, corresponding to the inversion of the real values ($R_1 < R_2$); it appears that, if there is a good accuracy for R_1—around 1.95 Å—there is a large minimum for R_2 from 2.00 to 2.30 Å, due to a weaker and thus less precise contribution. In the same way, we undertook to study the relationship between the number of neighbours and the Debye–Waller factor. The sets (N_1, σ_1) and (N_2, σ_2) are respectively shown in figures 7 and 8. For the two shells, the Debye–Waller factor is weakly determined and a result with almost all the values could be found. The variation in σ_i affects the number of neighbours but nevertheless, we observe that we do not have the same behaviour for N_1 and N_2: whatever the Debye–Waller value, N_1 remains in general above three and N_2 below.

A comparison with the results obtained for $KNbO_3$ leads to the following remarks.

—Two Nb–O distances are evidenced in the two compounds and there is no meaningful evolution of them in the temperature range 300–4 K.

—The shortest Nb–O distance is longer in PMN (1.95 Å) than in $KNbO_3$ (1.89 Å [1]). The longer distance is almost the same in PMN (2.16 Å) and in $KNbO_3$ (2.15 Å).

—The two populations of O neighbours are not equal; in $KNbO_3$, we have found three short and three long Nb–O bonds within the NbO_6 octahedron whereas in PMN there are

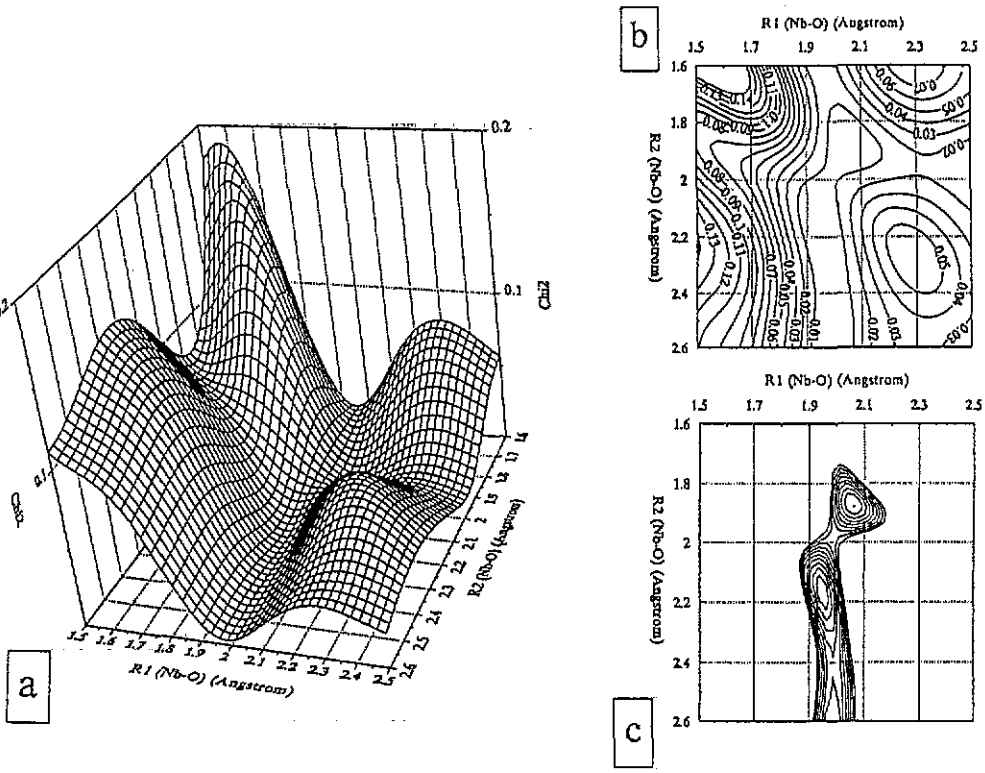

Figure 6. (*a*) Evolution of the χ^2 factor with the variation of the distances R_1 and R_2 for the first and second O shells respectively (R_1 from 1.5 to 2.5 Å and R_2 from 1.6 to 2.6 Å); (*b*) map of the 0.01 step variations of χ^2; (*c*) map of the χ^2 values lower than 0.01.

about four short and two long Nb–O bond lengths.

These differences can be explained by the presence of two cations Nb^{5+} and Mg^{2+} on the B site of the perovskite in PMN, originating different types of Nb neighbourhood and heterogeneities of composition as mentioned above.

As remarked previously, the nanostructure of PMN is made up of:

(1) Nanodomains of about 20 Å size in which Nb^{5+} and Mg^{2+} cations are 1–1 ordered on the B site of the perovskite. This ordering leads locally to a doubling of the perovskite unit cell parameter ($a \simeq 8$ Å) with $Fm3m$ space group. In these domains, no ferroelectricity is expected. Taking into account the difference in the chemical nature of the Mg^{2+} and Nb^{5+} cations, and more particularly their respective electronegativities (1.2 and 1.6 according to Pauling [14]) and ionic radii (0.72 Å and 0.64 Å according to Shannon and Prewitt [15]), the Nb–O bonds are expected to be shorter and more covalent than the Mg–O bonds. They should exhibit bond lengths close to those found in the [0.1 $PbMg_{1/3}Nb_{2/3}O_3$–0.9 $PbMg_{1/2}W_{1/2}O_3$] solid solution (0.1 PMN–0.9 PMW) [16] and in [$PbCo_{1/2}W_{1/2}O_3$] (PCW) [17] in which such a 1–1 order exists. In 0.1 PMN–0.9 PMW, Amin *et al* [16] showed that the O atoms undergo antiparallel displacements towards the smaller B cations (i.e. W(Nb) cations). The O octahedra about the W(Nb) and Mg(Nb) cations are regular but not equivalent. Thus, the metal–O bond lengths exhibit two values: Mg(Nb)–O bonds of 2.08 Å

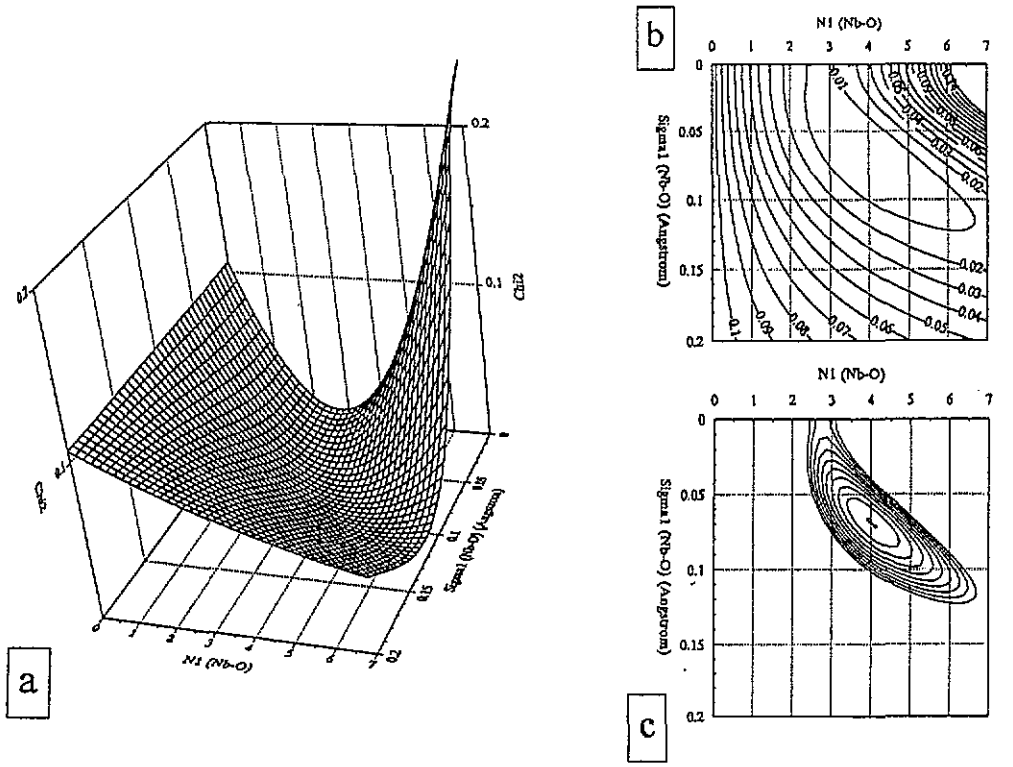

Figure 7. (*a*) Evolution of the χ^2 factor with the variation of the number of neighbours N_1 and the Debye–Waller factor σ_1 for the first O shell (N_1 from 0 to 7 and σ_1 from 0 to 0.2 Å); (*b*) map of the 0.01 step variations of χ^2; (*c*) map of the χ^2 values lower than 0.01.

and W(Nb)–O bonds of 1.93 Å. In the same way, Baldinozzi *et al* [17] give respectively lengths of 1.93 and 2.105 Å for W–O and Co–O in PCW.

(2) The host lattice, richer in Nb than the average composition, in which atoms could be shifted along ⟨111⟩ directions, originating three short and three long Nb–O bonds in each NbO_6 octahedron. As the temperature is lowered from 600 K the shifts correlate to give rise to polar nanodomains reaching a size of about 100 Å at very low temperatures. These nanodomains would exhibit a rhombohedral structure close to that of the rhombohedral phase of $KNbO_3$. In $KNbO_3$, the Nb–O bond lengths are respectively 1.89 and 2.15 Å. In PMN, two such types of bond (Nb→O–Mg) are also expected with a more complicated arrangement because of the presence of Mg atoms originating also Nb→O–Mg and Nb–O←Mg polar bonds. This should lead to different types of bond and thus different lengths for the Nb–O bonds.

EXAFS results show that there are only two types of Nb–O bond length. This result may be interpreted as follows.

—In the ordered domains, Nb–O bonds should have a length of 1.95 Å, which is quite satisfactory in comparison to the results of PMN–PMW and PCW.

—In the host lattice, it should exist short Nb–O bonds of 1.95 Å and longer ones of 2.15 Å. If we consider a shift of the Nb cation along a ⟨111⟩ direction in its octahedron,

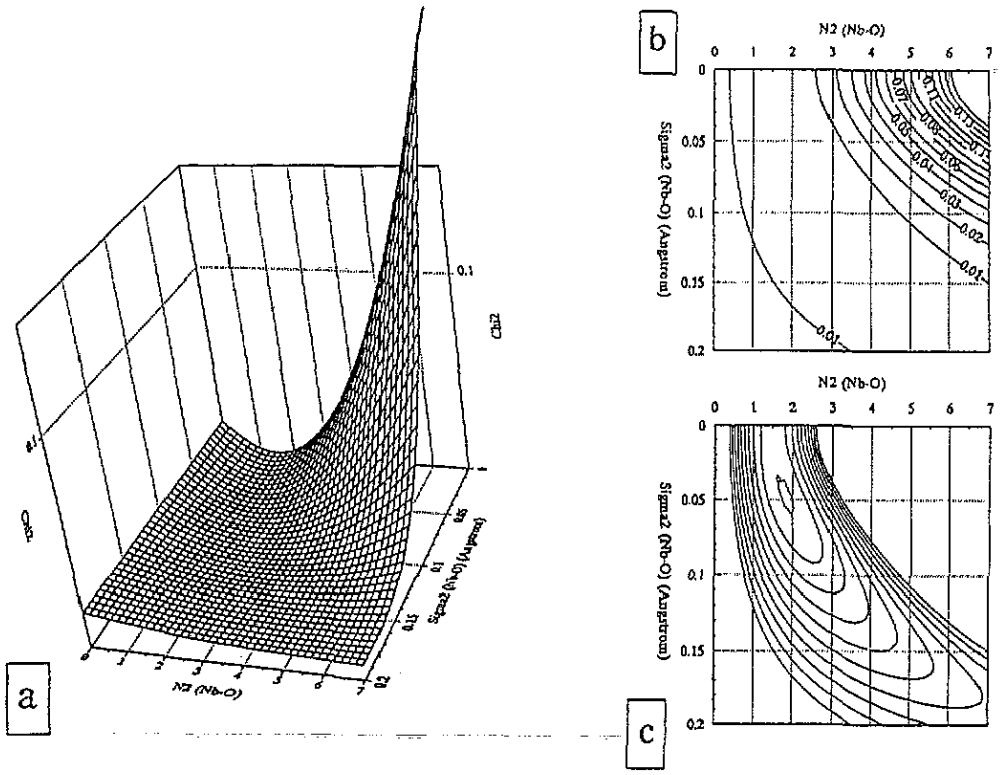

Figure 8. (*a*) Evolution of the χ^2 factor with the variation of the number of neighbours N_2 and the Debye–Waller factor σ_2 for the second O shell (N_2 from 0 to 7 and σ_2 from 0 to 0.2 Å); (*b*) map of the 0.01 step variations of χ^2; (*c*) map of the χ^2 values lower than 0.01.

considered as rigid, the shift is about 0.115 Å, comparable to the value of 0.126 Å found for $KNbO_3$. The fact that only two lengths of Nb–O bonds are observed shows that there are few Nb→O–Mg and Nb–O←Mg polar bonds; there should be thus a small content of Mg atoms that generally behave like Nb cations in the host lattice.

Now, if we consider the N_1 and N_2 values, in the 1–1 ordered domains, there are six short Nb–O bonds per NbO_6 octahedron whereas in the host lattice, there are approximately three short and three long Nb–O bonds per NbO_6 octahedron. The real structure corresponds to an average number of short bonds between three and six and of long bonds between zero and three. The values found here—about four bonds at 1.95 Å and two at 2.15 Å—are quite satisfactory. In the first approximation, this result leads to about one third ordered regions in the material and about two thirds disordered ones. Thus, approximately one half of the magnesium atoms should lie in the ordered regions with a chemical formula $PbMg_{1/2}Nb_{1/2}O_3$ and one half in the host lattice with a chemical formula close to $PbMg_{1/4}Nb_{3/4}O_3$.

This result is in good agreement with other work. Raman spectroscopy studies [11] have revealed the existence of polar Nb–O bonds with an Nb–O–Nb stretching frequency range at about 600 cm^{-1}. It exhibits a broad band at 300 K with two maxima at 570 and 510 cm^{-1}, which are better resolved at low temperature when the local ferroelectricity increases: they

Table 2. Results of the fits for the Nb/Mg shells. N_1 and R_1 represent respectively the number of Nb neighbours and the Nb–Nb distances. σ_1 and ΔE_1 are the Debye–Waller factor and the energy shift versus the experimental Nb K edge. N_2 and R_2 represent respectively the number of Mg neighbours and the Nb–Mg distances. σ_2 and ΔE_2 are the Debye–Waller factor and the energy shift versus the experimental Nb K edge. ρ and χ^2 are error factors. The fitting is performed with Teo and Lee's tabulated amplitude and phase shift files; S_0 (the scale factor) and Γ ($\Gamma = k/\lambda$ where λ is the electronic mean free path) are respectively fixed at 0.9 and 0.47 Å^{-2}.

	300 K	230 K	100 K	4.5 K
Niobium				
N_1 (fixed)	(4)	(4)	(4)	(4)
R_1 (Å)	3.88	3.93	3.93	3.92
σ_1 (Å)	0.09	0.09	0.09	0.08
ΔE_1^0 (eV)	1.0	0.6	6.2	6.7
Magnesium				
N_2 (fixed)	(2)	(2)	(2)	(2)
R_2 (Å)	4.00	3.89	3.89	4.00
σ_2 (Å)	0.02	0.09	0.00	0.00
ΔE_2^0 (eV)	2.7	1.1	6.5	5.3
ρ (%)	5.0	4.0	2.8	2.6
χ^2	0.6×10^{-3}	0.7×10^{-3}	0.8×10^{-3}	0.7×10^{-3}

are observed at 596 and 484 cm^{-1} at 4 K. Such B–O polar bonds have also been evidenced on the Raman spectra of $PbZr_xTi_{1-x}O_3$ compounds [18]. Moreover, the existence of 1–1 ordered regions with $Fm3m$ symmetry has been demonstrated by Siny and Boulesteix [12] through polarized Raman study of PMN crystals. Taking into account the intensity of the superstructure spots observed in the electron diffraction patterns, the ordered nanodomains exist in relatively important quantities in the material [9, 10]. This is confirmed by the high-resolution transmission electron microscopy images exhibiting numerous nanodomains with an 8 Å cell parameter. A numerical treatment of these images led to an ordered domains content of about 30% [19].

3.1.2. The niobium/magnesium shell. For the first Nb/Mg shell, the RDF given in figure 1 shows one well resolved peak. For the outer shell, the resolution is very poor, in comparison with that observed in $KNbO_3$. The intensity variation of these peaks in PMN compared to $KNbO_3$ reveals the occurrence of an important disorder on the perovskite B site. In addition, it can be observed, both in $KNbO_3$ and PMN, that the intensity of this peak increases when the temperature is lowered, whereas the O peak intensity remains quite constant. This observation may be linked to the increase of the atomic shift correlations with the temperature decreasing.

The fits were performed for the first Nb/Mg shell between 4.0 and 14.0 Å^{-1} on $k\chi(k)$ EXAFS spectra from a back Fourier transform taken from 3.10 to 4.20 Å. We took the same value as in our previous study for Γ ($\Gamma_1 = \Gamma_2 = 0.47$ Å^{-2}) and $S_0 = 0.9$ [1]. In order to simplify the calculations, we assumed that there is a statistical distribution of Nb and Mg atoms. In that case, each atom of Nb has on average four Nb and two Mg as first cationic neighbours. The results are given in table 2. The mapping of χ^2 factor versus the set (R_1, ΔE_1) for the Nb neighbourhood (figure 9) exhibits three mathematical minima but only the (3.9–4.0 Å; 0–8 eV) range has physical meaning, taking into account the previous results and considerations. For the Nb–Mg distances, many mathematically correct results

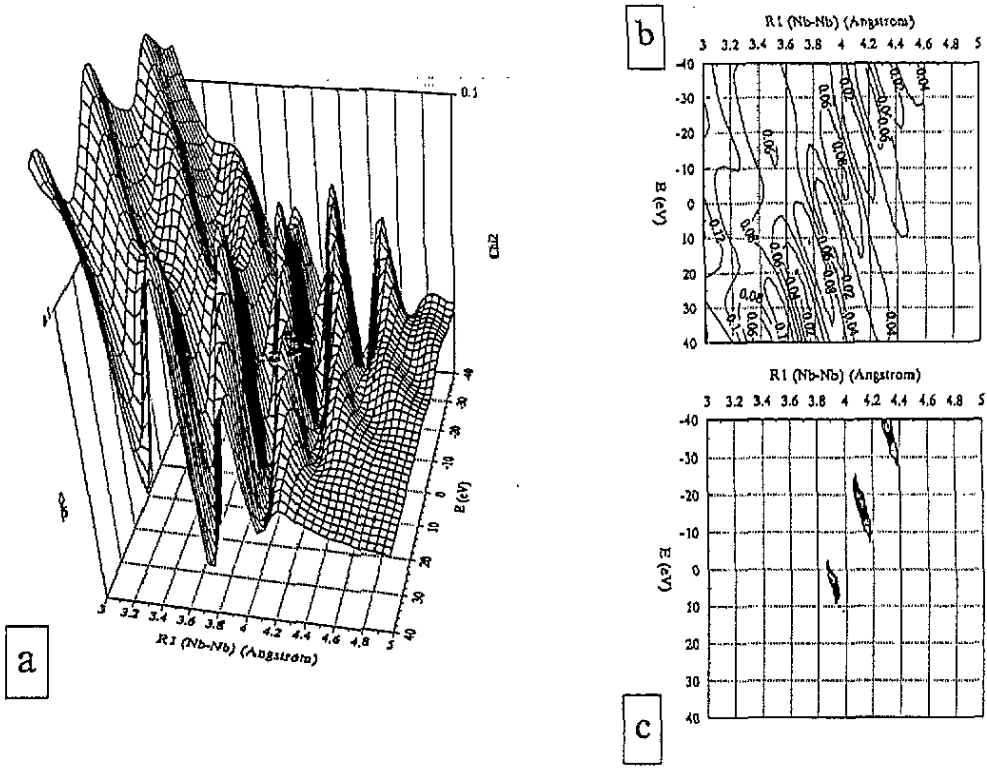

Figure 9. (*a*) Evolution of the χ^2 factor with the variation of the distance R_1 and the edge shift E for the Nb shell (R_1 from 3.0 to 5.0 Å and E from −40 to 40 eV); (*b*) map of the 0.02 step variations of χ^2; (*c*) map of the χ^2 values lower than 0.01.

can be found in a continuous set of R_2 values (figure 10). Thus, we cannot trust the result obtained through this fit process for the Mg neighbourhood.

3.2. *Lead L_{III} edge*

Figure 11 compares the RDFs of the PMN EXAFS spectra at 300 and 4.5 K with PbO and $PbTiO_3$ ones. This comparison shows that for PMN, there is no obvious EXAFS signal at the Pb L_{III} edge. This phenomenon cannot be due to thermal motion because the EXAFS contribution does not appear with decreasing temperature, even at 4.5 K. This result must be linked to the Nb K edge experiments for which we did not observe the Pb neighbourhood, in contrast to the K one for $KNbO_3$ (see figure 1). The absence of the Pb contribution must be explained by a large distribution in the atomic positions of Pb: it should give numerous distances which could not lead to a constructive EXAFS signal. Verbaere *et al* [8] have shown that the Pb atoms are shifted by 0.32 Å from their 'ideal' site with 24 disordered positions along directions close to (225). Our work confirms this result because such a static dispersion explains why (i) the Pb EXAFS signal is so small and (ii) the Pb shell can not be detected in the Nb edge EXAFS signal, even at low temperature.

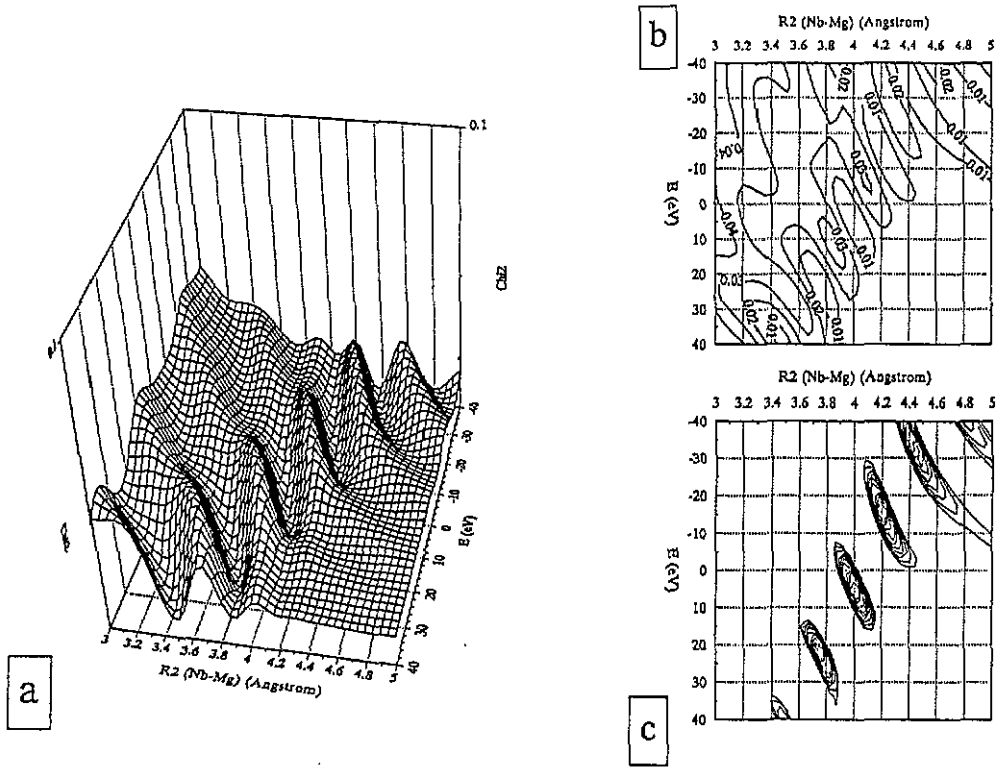

Figure 10. (*a*) Evolution of the χ^2 factor with the variation of the distance R_2 and the edge shift E for the Mg shell (R_2 from 3.0 to 5.0 Å and E from −40 to 40 eV); (*b*) map of the 0.01 step variations of χ^2; (*c*) map of the χ^2 values lower than 0.01.

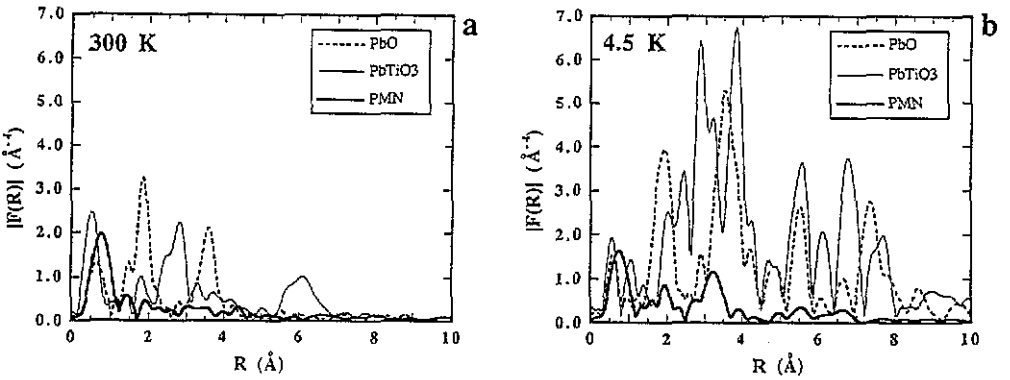

Figure 11. RDF (uncorrected for phase shift) of the $k\chi(k)$ data at the Pb L_{III} edge EXAFS spectra for the 300 K (*a*) and 4.5 K (*b*) samples (uncorrected for phase shift) for the PMN samples compared to $PbTiO_3$ and PbO. Due to disorder, no shell can be seen in the RDF of PMN. The lack of signal, even at 4.5 K, proves that this disorder is not thermal but static.

4. Conclusion

This EXAFS study has allowed us to determine the local order in PMN. Firstly two types of Nb–O bond have been demonstrated. Taking into account (i) the presence of two cations as chemically different as Nb^{5+} and Mg^{2+} on the B site of the perovskite and (ii) the existence of both Nb-rich polar nanodomains and Mg-rich 1–1 ordered nanodomains, the result can seem quite surprising. If we consider the present results and those obtained by other techniques, we can say that about one third of the material should consist of ordered domains with $Fm3m$ symmetry exhibiting regular NbO_6 octahedra (Nb–O bond length of 1.95 Å) and larger MgO_6 octahedra. The host lattice should present a chemical composition close to $PbMg_{1/4}Nb_{3/4}O_3$ where the polar nanodomains progressively nucleate: Nb shifts along a ⟨111⟩ cubic axis give rise to Nb–O bond lengths of 1.95 and 2.16 Å.

The Nb–Nb and Nb–Mg distances are in good agreement with the structural data obtained by x-ray and neutron diffraction [6, 8]. However, the increase of intensity of the Nb–Ng(Mg) peak on the RDF when the temperature is lowered confirms the progressive correlation of the Nb shifts originating the polar domain growth. It is indeed well known that EXAFS signals are very sensitive to disorder. It can be noted that the intensity of this peak increases by about 50% between 300 and 100 K but does not grow further below this temperature. This observation confirms our previous structural studies that have revealed that the structure seems to freeze below 100 K [9].

Finally, the lack of a significant EXAFS signal, both at the Nb edge for the Pb shell and at the Pb edge for the local order around Pb^{2+} cations, confirms the very important disorder of the Pb atomic positions, also revealed by x-ray diffraction results [8].

References

[1] de Mathan N, Prouzet E, Husson E and Dexpert H 1993 *J. Phys.: Condens. Matter* **5** 1261
[2] Comes R, Lambert M and Guinier A 1968 *Solid State Commun.* **6** 715
[3] Comes R, Lambert M and Guinier A 1970 *Acta Crystallogr.* **26** 244
[4] Sokoloff J P, Chase L L and Rytz D 1988 *Phys. Rev.* B **38** 597
[5] Bonneau P, Garnier P, Husson E and Morell A 1989 *Mater. Res. Bull.* **24** 201
[6] Bonneau P, Garnier P, Calvarin G, Husson E, Gavarri J R, Hewat A W and Morell A 1991 *J. Solid State Chem.* **91** 350
[7] de Mathan N, Husson E, Calvarin G, Gavarri J R, Hewat A W and Morell A 1991 *J. Phys.: Condens. Matter* **3** 8159
[8] Verbaere A, Piffard Y, Ye Z G and Husson E 1992 *Mater. Res. Bull.* **27** 1227
[9] de Mathan N, Husson E and Morell A 1992 *Mater. Res. Bull.* **27** 867
[10] Husson E, Chubb M and Morell A 1988 *Mater. Res. Bull.* **23** 357
[11] Husson E, Abello L and Morell A 1990 *Mater. Res. Bull.* **25** 539
[12] Siny I and Boulesteix C 1989 *Ferroelectrics* **96** 119
[13] *Teo B K and Lee P A 1979 J. Am. Chem. Soc.* **101** 2815
[14] Pauling L 1967 *The Chemical Bond* (Ithaca: Cornell University Press)
[15] Shannon R D and Prewitt C T 1969 *Acta Crystallogr.* B **25** 925
[16] Amin A, Newnham R E, Cross L E, Nomura S and Cox D E 1980 *J. Solid State Chem.* **35** 267
[17] Baldinozzi G, Sciau P and Lapasset J 1993 *Phys. Status Solidi* at press
[18] Husson E, Repelin Y, Abello L and Lucazeau G 1984 *9th Int. Conf. on Raman Spectroscopy (Tokyo)*
[19] Boulesteix C, Varnier F, Lieberia A and Husson E *J. Solid State Chem.* at press